

# Supplementary material

## GPU Accelerated 3D Tomographic Reconstruction and Visualization from Noisy Electron Microscopy Tilt-Series

Julio Rey Ramirez, Peter Rautek, Ciril Bohak, Ondřej Strnad, Zheyuan Zhang, Sai Li, Ivan Viola, and Wolfgang Heidrich, *Fellow, IEEE*,

### 1 GAUSSIAN DENOISERS AS PROXIMAL OPERATORS

Any Gaussian denoiser can be interpreted as a proximal operator as seen in the works by Venkatakrishnan *et al.* [1] and Heide *et al.* [2]. Assuming that the volumes present Gaussian noise with standard deviation  $\sigma_{nlm}$ , the likelihood of an observed volume  $b$  given a latent volume  $v$  is:

$$f(b|v) \propto \exp\left(-\frac{\|b-v\|_2^2}{2\sigma_{nlm}^2}\right). \quad (1)$$

Assuming some prior distribution  $G(v)$ , the maximum a posterior estimate (MAP) of the intrinsic volume is:

$$\begin{aligned} v_{MAP} &= \arg \max_v G(v) \cdot f(b|v), \\ &= \arg \min_v -\log(G(v)) + \frac{1}{2\sigma_{nlm}^2} \|b-v\|_2^2. \end{aligned}$$

By defining  $\tilde{G}(v) = -\log(G(v))$ , the expression above has the form of the definition of proximal operator [3], and then

$$v_{MAP} = \text{prox}_{\sigma_{nlm}^2 \tilde{G}}(b) \quad (2)$$

The prior distribution  $g(v)$  may not be known, but it can be an implicit assumption in denoising algorithms. With this, any Gaussian denoiser that can be formulated as a MAP estimation can be interpreted as a proximal operator with fixed regularization parameter as the assumed variance of the noise  $\sigma_{nlm}^2$ .

### 2 HORIZONTAL PADDING FOR LIMITED ANGLE RECONSTRUCTIONS

Let  $vd$  be the volume depth and  $pw$  the projection width. The volume width including the required padding corresponds to  $2(x+y)$ , where  $x$  is the horizontal distance from the center of the volume to the intersection of the purple ray

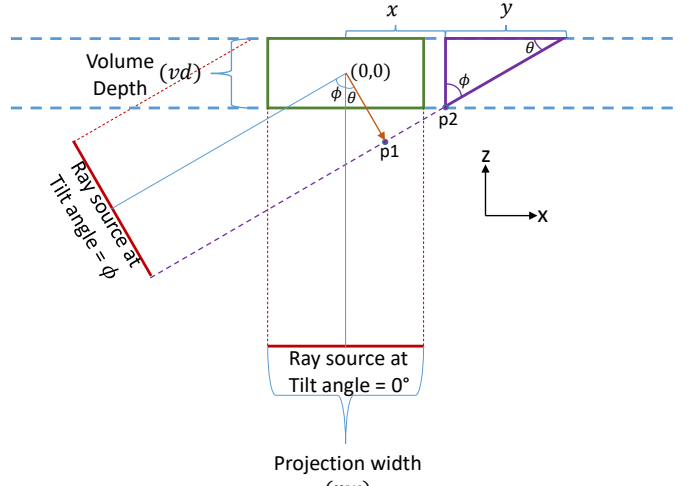


Fig. 1. Top view of the reconstruction scene. Horizontal padding is required for the extreme views.

with the horizontal line  $z = -\frac{vd}{2}$ , and  $y$  is the horizontal distance from the intersection of such ray with  $z = -\frac{vd}{2}$  to the intersection with  $z = \frac{vd}{2}$ .  $y$  can be computed from the purple triangle with angles  $\phi$  (corresponding to maximum tilt angle) and  $\theta = 90 - \phi$

$$y = \frac{vd}{\tan(\theta)} \quad (3)$$

To find  $x$ , we need to find the intersection of the purple ray with  $z = -\frac{vd}{2}$ . For this, we assume that the center of the volume is located at  $(0, 0)$ . Then, we move from the origin to  $p1$ , moving  $\frac{pw}{2}$  along the  $(\sin(\theta), -\cos(\theta))$  direction.

$$\vec{p1} = \frac{pw}{2} \cdot (\sin(\theta), -\cos(\theta)) \quad (4)$$



Fig. 2. IsoNet bin-3 vs bin-8

Then, we cast a ray from  $\vec{p_1}$  to  $\vec{p_2}$

$$\vec{p_1} + t \cdot (\cos(\theta), \sin(\theta)) = (x, -\frac{vd}{2}) \quad (5)$$

solving for  $t$  from the  $z$  components

$$t = \frac{-\frac{vd}{2} + \cos(\theta) \frac{pw}{2}}{\sin(\theta)} \quad (6)$$

now, we can use  $t$  to find  $x$

$$x = \frac{pw}{2} \sin(\theta) + \frac{-\frac{vd}{2} + \cos(\theta) \frac{pw}{2}}{\sin(\theta)} \cos \theta \quad (7)$$

and finally, the volume width  $vw$  including padding is

$$vw = 2|x| + y \quad (8)$$

$$= |pw \cdot \sin(\theta) + (pw \cdot \cos(\theta) - vd) \cdot \cot(\theta)| + \frac{2vd}{\tan(\theta)} \quad (9)$$

### 3 ISO NET BIN-3 VS BIN-8

When using IsoNet for tomogram refinement, the authors recommended that the tilt-series are binned so that the reconstructed volumes have a pixel size of around 10 Å [4]. However, in order to compare line profile results between IMOD, ours and IsoNet, we created reconstructions at a higher resolution (bin 3, pixel size 3.537 Å) that was used for reconstruction using IMOD and our approach. Figure 2 includes a comparison between IMOD, IsoNet bin-3 and IsoNet bin-8 results. When using higher resolution (bin-3), IsoNet produces results very similar to IMOD's. Using the recommended bin-3 setting, IsoNet achieves good denoising results, but the final resolution is much lower.

### 4 COMPARISON WITH MBIR IN THE ORTHOGONAL SLICES

Additional images comparing our technique and MBIR [5] in the orthogonal slices. Central XZ slice Figure 3 and central XY slice Figure 4.

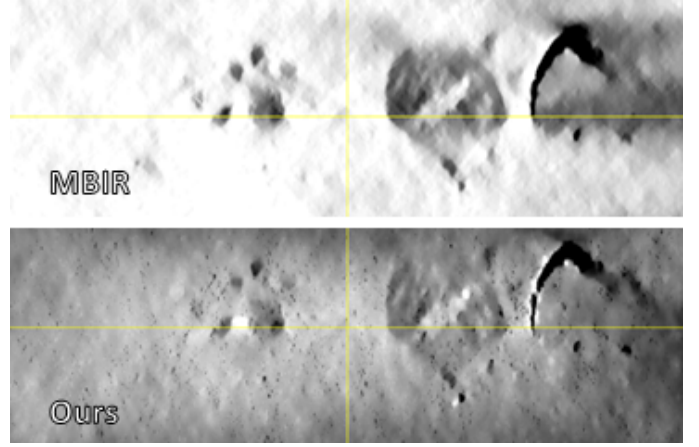


Fig. 3. Comparison between our method and MBIR on the central XZ reconstructed slice for the ablation dataset.

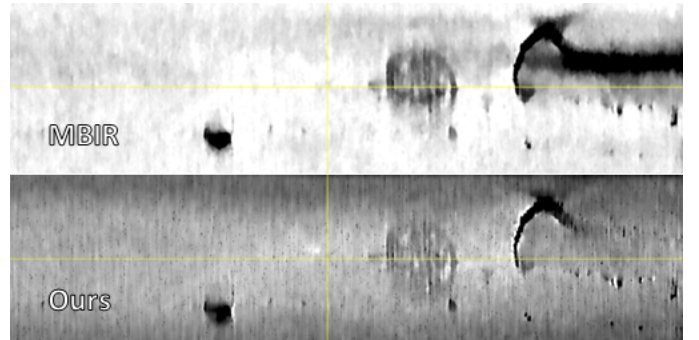


Fig. 4. Comparison between our method and MBIR on the central YZ reconstructed slice for the ablation dataset.

### 5 TV VS. HUBER PENALTY

Figure 5 includes comparisons between TV+NLM and Huber+TV for more datasets. In the HIV and Influenza (top and bottom) datasets TV+NLM results present less background noise. In the SARS-CoV-2 (middle), Huber+NLM produced more homogeneous results in comparison with TV+NLM, which presents white dots.

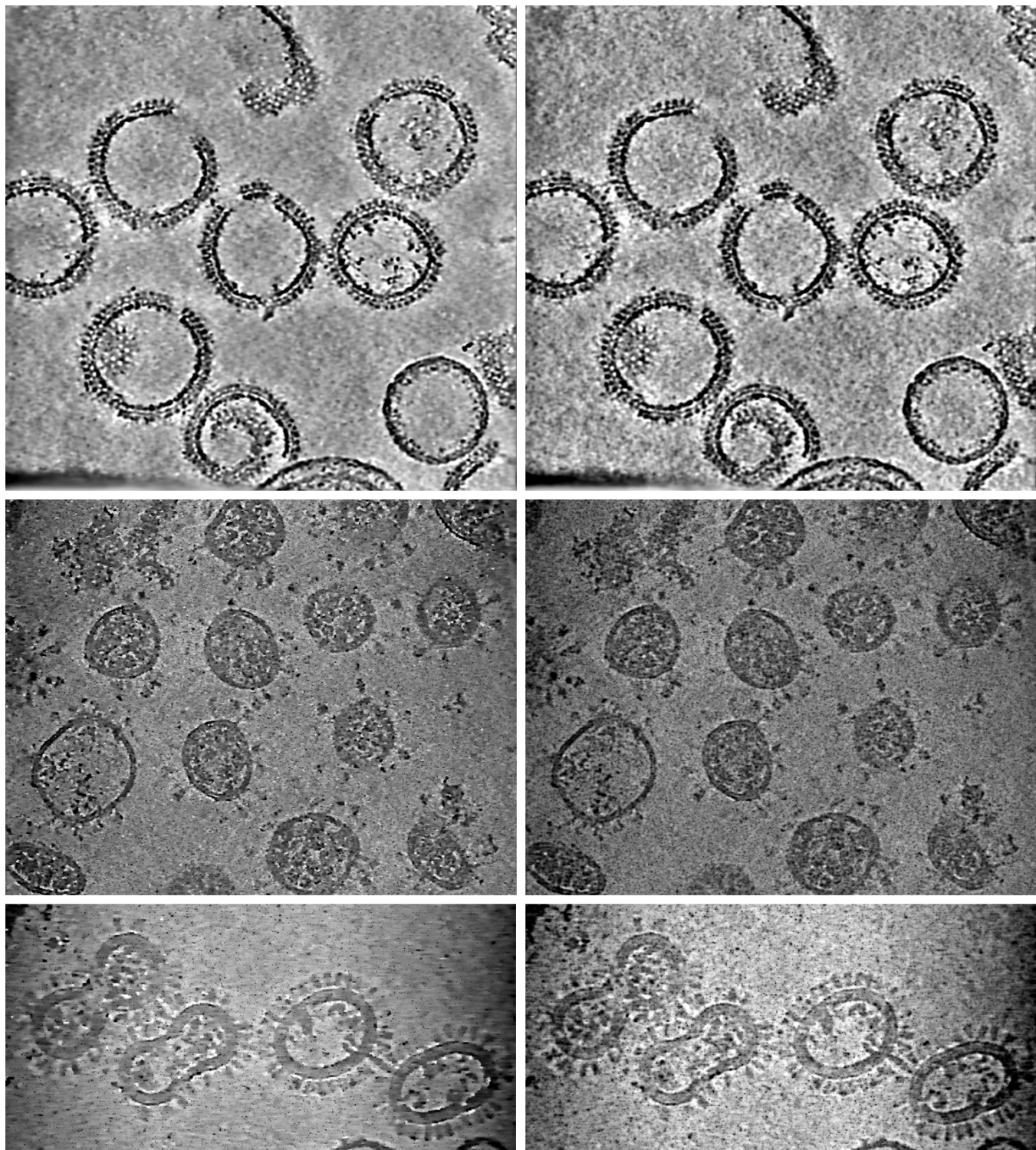


Fig. 5. TV+NLM (left) vs. Huber+NLM (right).

## 6 MASKING THE FIDUCIALS

Additional images (Figure 6, Figure 7, Figure 8) illustrating the effects of masking the fiducials to ignore the pixels corresponding to fiducial markers during the reconstruction process.

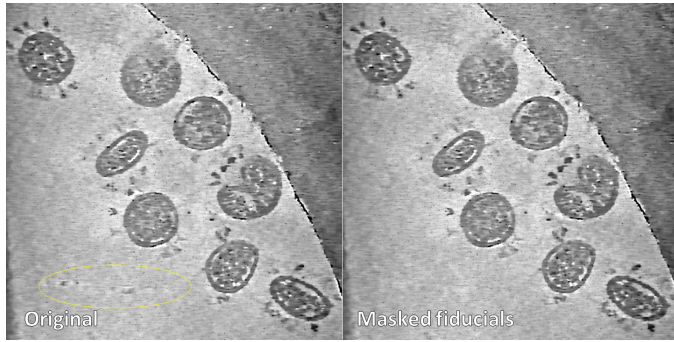


Fig. 6. Original vs masked fiducials on the dataset used in the ablation study.

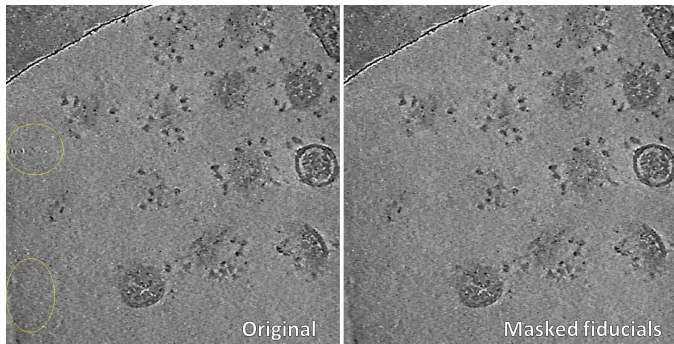


Fig. 7. Original vs masked, on the dataset used for the progress over time evaluation.

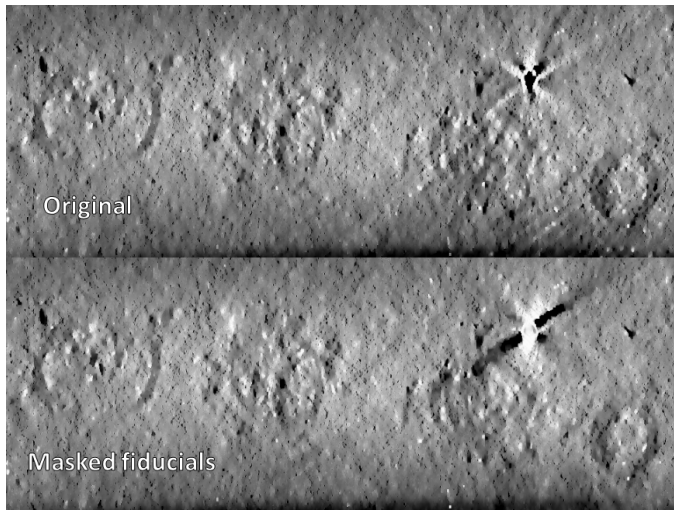


Fig. 8. Original vs masked, XZ slice on the dataset used for the progress over time evaluation.

## 7 ADDITIONAL ITERATIONS FOR DATASET 2

Figure 9 corresponds to reconstructions of dataset 2 up to  $3 \times 100$  iterations. TV was used for the first 98 proximal

iterations, and TV+NLM was used for the last 2.

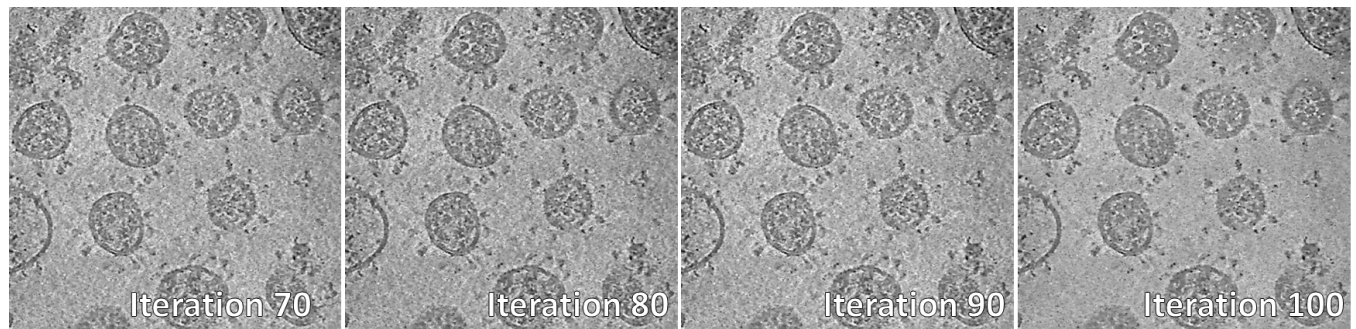


Fig. 9. Reconstruction progress from SARS-CoV-2 tilt-series (dataset 2).  $3 \times 100$  iterations. First 98 with TV regularization, last two using TV+NLM

## REFERENCES

- [1] S. V. Venkatakrishnan, C. A. Bouman, and B. Wohlberg, "Plug-and-play priors for model based reconstruction," *2013 IEEE Global Conference on Signal and Information Processing*, pp. 945–948, 2013.
- [2] F. Heide, M. Steinberger, Y. Tsai, M. Rouf, D. Pajak, D. Reddy, O. Gallo, J. Liu, W. Heidrich, K. Pajak, J. Kautz, and K. Pulli, "FlexISP: A Flexible Camera Image Processing Framework," *ACM Transactions on Graphics (Proc. SIGGRAPH Asia)*, 2014.
- [3] N. Parikh and S. Boyd, "Proximal Algorithms," *Foundations and Trends in Optimization*, vol. 1, no. 3, pp. 127–239, Jan. 2014.
- [4] Y.-T. Liu, H. Zhang, H. Wang, C.-L. Tao, G.-Q. Bi, and Z. H. Zhou, "Isotropic Reconstruction of Electron Tomograms with Deep Learning," *bioRxiv*, jul 2021.
- [5] R. Yan, S. V. Venkatakrishnan, J. Liu, C. A. Bouman, and W. Jiang, "MBIR: A Cryo-ET 3D Reconstruction Method that Effectively Minimizes Missing Wedge Artifacts and Restores Missing Information," *Journal of structural biology*, vol. 206, no. 2, pp. 183–192, May 2019.